A volume-averaged model for acoustic streaming induced by focused ultrasound in soft porous media

Sebastian E. N. Price,[1] Rune Hansen,[2] and Magnus Aa. Gjennestad[3]
[1)] *PoreLab and Department of Chemistry at The Norwegian University of Science and Technology (NTNU), Trondheim, Norway*[a]
[2] *Department of Health Research at SINTEF and Department of Circulation and Medical Imaging at The Norwegian University of Science and Technology (NTNU), Trondheim, Norway*[b]
[3] *PoreLab and SINTEF Energy Research, Trondheim, Norway*[c]

(Dated: 23 June 2023)

Equations describing acoustic streaming in soft porous media driven by focused ultrasound are derived based on the assumption that acoustic waves pass through the porous material as if it were homogeneous. From these equations, a model that predicts the time-averaged flow on the macroscopic scale as well as the advective transport of the trace components is created. The model is used to perform simulations for different shapes of the focused ultrasound beam. For a given shape, and using the paraxial approximation for the ultrasound, the acoustic streaming is found to be linearly proportional to the applied ultrasound intensity, to the permeability of the porous material and to the attenuation coefficient, and inversely proportional to the liquid viscosity. Results from simulations are compared to a simplified expression stating that the dimensionless volumetric liquid flux is equal to the dimensionless acoustic radiation force. This approximation for the acoustic streaming is found to be reasonable near the beam axis for focused ultrasound beam shapes that are long in the axial direction, compared to their width. Finally, a comparison is made between the model and experimental results on acoustic streaming in a gel, and good agreement is found.

Author accepted manuscript version of article in
The Journal of the Acoustical Society of America 154 (2023). DOI: 10.1121/10.0020146.

I. INTRODUCTION

In the treatment of cancer, ultrasound has been found to improve the delivery of therapeutic agents into tumors, thereby improving the therapeutic response (Snipstad *et al.*, 2021). There are many proposed mechanisms for this improvement, among them is acoustic streaming which is the net movement of fluid generated by propagation of sound waves (Afadzi *et al.*, 2020; Nieminen *et al.*, 2012, 2015; Raghavan, 2018). However, to understand and assess the role of acoustic streaming, and to compare its effect relative to other possible mechanisms for improved delivery, it would be of great advantage to have an experimentally validated model.

The extracellular matrix of a tumor, which consists of a collagen network embedded in a gel of glycosaminoglycans, can be considered a porous medium (Snipstad *et al.*, 2021). We will therefore in this work derive equations describing acoustic streaming in soft porous media driven by focused ultrasound. The derivations are based on the assumption that acoustic waves pass through the porous material as if it were homogeneous. The resulting equations for the time-averaged flow on the macroscopic scale are, even though they represent a different physical situation, on the same form as Darcy's law (Whitaker, 1986) for an incompressible flow field. These equations seem to be a natural extension of Darcy's law to the case of acoustic streaming. They do not seem, however, to have been employed very often in the literature. We are also not aware of any previously published detailed derivation of these equations such as the one presented here. Presentation of the derivation is important because it makes the physical interpretation of the variables involved and the underlying assumptions clear and thus makes it possible to test the model and its assumptions against experiments.

Since one of the main motivations for studying acoustic streaming in soft, porous media is its potential impact on transport of drugs in tissue, we also include a time- and volume-averaged equation for advective transport of trace components.

There have been other recent contributions to the theoretical description of acoustic streaming in soft porous media from e.g. Raghavan (2018), Wessapan and Rattanadecho (2020), Manor (2021) and Yuan (2022). Interestingly, our equations are not the same as those of Raghavan (2018). While he emphasizes the importance of a conservation force, this term is not present in our equations. This stems from a different assump-

[a)] sebastian.n.price@ntnu.no
[b)] rune.hansen@sintef.no
[c)] magnus.gjennestad@sintef.no

tion about the second-order velocity of the solid phase and constitutes an important difference, since the conservation force is stated to be a dominating factor in Raghavan (2018) and Yuan (2022). Raghavan (2018) compared his model to results from different experiments on ultrasound-enhanced delivery in tissue and obtained fair agreement in some cases, e.g., when comparing it to the results of Lewis *et al.* (2012) and Olbricht *et al.* (2013) for ultrasound-assisted convection-enhanced delivery to the brain of rodents. Yuan (2022) derived a model for acoustic streaming in soft porous media, which includes a conservation force similar to that in Raghavan (2018). Furthermore, he proposed a new mechanism, the *squeezing interstitial fluid via transfer of ultrasound momentum*, to be the main contributor to the streaming. By this mechanism, the ultrasound beam generates interstitial fluid streaming from squeezing the tissue in the focal volume. Wessapan and Rattanadecho (2020) numerically calculated the acoustic streaming field in a porous tissue during exposure to high-intensity focused ultrasound by employing the Brinkman-extended Darcy model (Brinkman, 1949). They did not, however, go into any details on how they arrived at their equations. Manor (2021) presented a comprehensive theoretical treatment where he considers the effect of wavelength with respect to pore size and the effect of similar and different acoustic properties in the fluid and solid phases. His equations were, however, based on flow in tubes and therefore not as general as those presented here. A formal volume-averaging approach, such as the one used here, was not applied.

Manor (2021) suggested a simplified equation to estimate the acoustic streaming which can be evaluated directly from knowledge of the acoustic radiation force and does not require the solution of a partial differential equation. In practice, the same approach was also used by Afadzi *et al.* (2020) and Løvmo *et al.* (2020). They used a Darcy-type equation to estimate the acoustic streaming, but replaced the pressure gradient with the acoustic radiation force as the only driving force for the flow. In our work, we test the validity of this simplified approach against numerical solutions to the derived model equations and provide new insight as to when the approximation is valid and when it is not.

There is a decent amount of literature on experiments studying ultrasound-enhanced delivery in tissue. However, to use these to validate a model is often difficult. One reason for this difficulty is that tissue properties, such as permeability and porosity, are not always known accurately for the particular samples used in the experiments. They may also vary considerably between different samples, making it difficult to look them up from other sources. For the purposes of validating a model, it is of great advantage to have experimental results from a more controlled environment where important model parameters are independently measured. El Ghamrawy *et al.* (2019) performed experiments studying acoustic streaming induced by focused ultrasound of different intensities in a macroporous gel. The porosity and permeability of the gel was independently measured. We show that the model derived here agrees with the experimental results of El Ghamrawy *et al.* (2019). This is, as far as we know, the first comparison of a model for acoustic streaming in soft porous media with results from experiments in an environment with this level of control.

The rest of the article is structured as follows. In Section II we derive equations for the time-averaged acoustic streaming on the macroscopic scale. In Section III we briefly comment on the numerical solution procedures used to solve the equations and, in Section IV, we present results from simulations and comment on the validity of the simplified equation from e.g. Manor (2021). Finally, in Section V, we compare the experimental results of El Ghamrawy *et al.* (2019) to results from our model and, in Section VI, we conclude.

II. ACOUSTIC STREAMING IN A POROUS MEDIUM

We will here derive the equations necessary to describe acoustic streaming, and the associated advective transport of trace components, through a general soft porous medium driven by focused ultrasound. In Section V we will apply the equations on the specific case of a macroporous gel. At the pore scale, we distinguish between the solid phase (s), the liquid phase (ℓ) and their interface (ℓs). This is illustrated in FIG. 1. On this scale, the fluid flow is governed by well-known equations for mass conservation and momentum balance, see e.g. (Landau and Lifshitz, 1987). However, to solve these equations and thus resolve the interstitial flow through every pore in, e.g., the extracellular matrix of a large piece of tissue, is impractical and computationally difficult. The same is true for a piece of gel that is large compared to the pore size. We will therefore first derive the equations that describe the steady-state, time averaged flow of liquid on the pore scale and, thereafter, perform a volume averaging of the pore-scale equations and treat the porous medium as a continuum. The volume averaging procedure is a widely adopted strategy in porous media science (Gjennestad *et al.*, 2020; Whitaker, 1985, 1986).

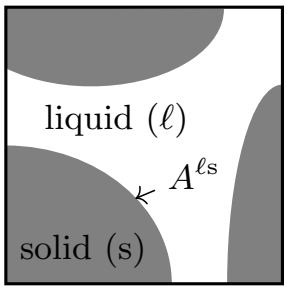

FIG. 1. Illustration of a porous material at the pore scale indicating the solid phase (s), the liquid phase (ℓ) and the liquid-solid interfacial area $A^{\ell s}$.

A. Acoustic streaming on the pore scale

In this section we will derive the equations that describe acoustic streaming on the pore scale, i.e., the flow field inside the pore space. The goal is to arrive at equations for time-averaged, steady-state fluid flow that can be volume-averaged in Section II B 2. We will start with some general considerations and then proceed with the conservation of mass and the balance of momentum.

To discuss sound propagation and acoustic streaming, we employ the well-established (Lighthill, 1978; Nyborg, 1953) perturbation approach and expand the fluid density, pressure and velocity as, respectively,

$$\rho = \rho_0 + \rho_1 + \rho_2 + ..., \tag{1}$$
$$p = p_0 + p_1 + p_2 + ..., \tag{2}$$
$$\mathbf{v} = \mathbf{v}_1 + \mathbf{v}_2 + ... \tag{3}$$

The constants ρ_0 and p_0 represent the undisturbed equilibrium state with no acoustic waves and no flow. The density ρ_1, pressure p_1 and velocity $\mathbf{v}_1$ are the first-order disturbances due to the acoustic wave. We assume here that these average to zero over a whole number of periods.

The acoustic streaming is represented by terms in the mass flux $\rho\mathbf{v}$ which are non-zero after time-averaging over a whole number of periods of the sound field oscillations. Keeping terms up to second order, the time-averaged mass flux is

$$\overline{\rho\mathbf{v}} = \frac{1}{\tau}\int_{-\tau/2}^{\tau/2} \rho\mathbf{v}\ \mathrm{d}t = \overline{\rho_1\mathbf{v}_1} + \rho_0\bar{\mathbf{v}}_2. \tag{4}$$

We have here used that the first-order term $\rho_0\bar{\mathbf{v}}_1$ will be zero and the net mass flux is therefore represented by the two second-order terms.

While there is acoustic streaming of the liquid phase, the time-averaged mass flow of solid must vanish in steady state. We can employ a similar expansion as shown in (1) and (3) for the solid and the second-order mass flux then has the same form as (4),

$$\overline{\rho^{\mathrm{s}}\mathbf{v}^{\mathrm{s}}} = \overline{\rho_1^{\mathrm{s}}\mathbf{v}_1^{\mathrm{s}}} + \rho_0^{\mathrm{s}}\bar{\mathbf{v}}_2^{\mathrm{s}} = \mathbf{0}. \tag{5}$$

The second-order solid velocity must therefore be

$$\bar{\mathbf{v}}_2^{\mathrm{s}} = -\frac{\overline{\rho_1^{\mathrm{s}}\mathbf{v}_1^{\mathrm{s}}}}{\rho_0^{\mathrm{s}}}. \tag{6}$$

The intensity of the acoustic field is the time-average of $p_1\mathbf{v}_1$,

$$\mathbf{I} = \overline{p_1\mathbf{v}_1}. \tag{7}$$

1. Conservation of total liquid mass

Conservation of total mass, i.e., the sum of all chemical components, in a compressible liquid is described by (Landau and Lifshitz, 1987)

$$\partial_t\{\rho\} + \nabla\cdot\{\rho\mathbf{v}\} = 0. \tag{8}$$

We insert the perturbation expansion, (1) and (3), and gather terms of first and second order. Subsequently, we take the time average of the resulting second-order equation and get

$$\nabla\cdot\bar{\mathbf{v}}_2 = -\frac{\nabla\cdot\overline{\rho_1\mathbf{v}_1}}{\rho_0}. \tag{9}$$

In subsequent analysis we will use the velocity field $\bar{\mathbf{u}}_2$ defined by

$$\bar{\mathbf{u}}_2 = \bar{\mathbf{v}}_2 + \frac{\overline{\rho_1\mathbf{v}_1}}{\rho_0}. \tag{10}$$

This is convenient because inserting it into (9), we immediately get that

$$\nabla\cdot\bar{\mathbf{u}}_2 = 0, \tag{11}$$

i.e. that $\bar{\mathbf{u}}_2$ is incompressible. Furthermore, the time-averaged fluid mass flux in (4) becomes

$$\overline{\rho\mathbf{v}} = \rho_0\bar{\mathbf{u}}_2, \tag{12}$$

when expressed in terms of $\bar{\mathbf{u}}_2$.

2. Balance of momentum

Balance of momentum for a compressible fluid may be expressed as (Landau and Lifshitz, 1987)

$$\partial_t\{\rho\mathbf{v}\} - \mathbf{F} = -\nabla p + \left\{\xi + \frac{1}{3}\eta\right\}\nabla\{\nabla\cdot\mathbf{v}\} + \eta\nabla^2\mathbf{v}, \tag{13}$$

where η the dynamic viscosity and ξ the bulk viscosity. The momentum flux term is written as $\mathbf{F} = -\rho\mathbf{v}\{\nabla\cdot\mathbf{v}\} - \mathbf{v}\nabla\cdot\{\rho\mathbf{v}\}$. We now insert the perturbation expansion (1)–(3) into the momentum equation (13). Gathering the second-order terms, and taking the time average, yields the second-order momentum equation

$$\nabla\bar{p}_2 - \bar{\mathbf{F}}_2 = \left\{\xi + \frac{1}{3}\eta\right\}\nabla\{\nabla\cdot\bar{\mathbf{v}}_2\} + \eta\nabla^2\bar{\mathbf{v}}_2, \tag{14}$$

where $\bar{\mathbf{F}}_2$ is the acoustic radiation force. Subsequently, using (9) and introducing $\bar{\mathbf{u}}_2$ in place of $\bar{\mathbf{v}}_2$ gives

$$\nabla\bar{p}_2 - \bar{\mathbf{F}}_2 - \eta\nabla^2\bar{\mathbf{u}}_2 = -\frac{1}{\rho_0}\left\{\xi + \frac{1}{3}\eta\right\}\nabla\{\nabla\cdot\overline{\rho_1\mathbf{v}_1}\} - \frac{\eta}{\rho_0}\nabla^2\overline{\rho_1\mathbf{v}_1}. \tag{15}$$

By some order-of-magnitude arguments, it is possible to show that the terms on the right hand side are expected to be relatively small for focused ultrasound in tissue-like materials. We then get

$$\nabla\bar{p}_2 - \bar{\mathbf{F}}_2 - \eta\nabla^2\bar{\mathbf{u}}_2 \approx \mathbf{0}. \tag{16}$$

3. Conservation of liquid component masses

The liquid may be considered a mixture of different chemical components. For purely advective transport, with no diffusion, the mass conservation equation for component i in the mixture is

$$\partial_t \left\{\rho z^i\right\} + \nabla \cdot \left\{\rho z^i \mathbf{v}\right\} = 0, \tag{17}$$

where z^i is the mass fraction of component i.

We now insert the perturbation expansions of $\mathbf{v}$ (3) and ρ (1), discard resulting terms of order larger than two, use the expanded mass equation (8), and get

$$\{\rho_0 + \rho_1 + \rho_2\}\partial_t \left\{z^i\right\} + \{\rho_0 \mathbf{v}_1 + \rho_1 \mathbf{v}_1 + \rho_0 \mathbf{v}_2\} \cdot \nabla z^i = 0. \tag{18}$$

Next, we apply time-averaging over a whole number of periods of the acoustic oscillations. We assume that variations in z^i are slow with respect to the period of the oscillations. The derivatives of z^i can therefore be approximated as constant in the time-averaging. Also using (10) to eliminate $\bar{\mathbf{v}}_2$, the time-averaged mass equation for component i becomes

$$\{\rho_0 + \bar{\rho}_2\}\partial_t \left\{z^i\right\} + \rho_0 \bar{\mathbf{u}}_2 \cdot \nabla z^i = 0. \tag{19}$$

Since $\bar{\mathbf{u}}_2$ is incompressible and $\bar{\rho}_2 \ll \rho_0$, this can also be expressed in conservation form as

$$\partial_t \left\{\rho_0 z^i\right\} + \nabla \cdot \left\{\rho_0 z^i \bar{\mathbf{u}}_2\right\} = 0. \tag{20}$$

The transport of component i in the pore space due to acoustic streaming may thus be approximated by an equation on the same form as (17). Note, however, that it is the divergence-free velocity $\bar{\mathbf{u}}_2$ which enters (20) and not the second-order velocity $\bar{\mathbf{v}}_2$.

B. Upscaling approach to porous media

In this section, we derive the continuum equations for acoustic flow in a porous medium. To obtain these from the pore-scale equations in Section II A, we first make use of the assumption of an acoustically homogeneous medium and then apply volume-averaging.

1. Homogeneous medium assumption

We make use of the key assumption that the acoustic waves, i.e. the first-order fields, propagate through the porous material as if it were a homogeneous material. This assumption was also employed by Raghavan (2018) and Manor (2021) and was called *imaging community assumption* in the work of Raghavan (2018) and was called the special case of *equal acoustic properties* by Manor (2021). The phase velocity c_0 and the acoustic impedance $Z = \rho_0 c_0$ are then assumed the same in the solid and the fluid. This means that $\rho_0 = \rho_0^{\mathrm{s}}$ and $\mathbf{v}_1 = \mathbf{v}_1^{\mathrm{s}}$ (Manor, 2021). Another consequence is that the no-slip condition on the liquid-solid boundary implies that

$$\bar{\mathbf{u}}_2 = \mathbf{0}, \text{ on } A^{\ell \mathrm{s}}. \tag{21}$$

This result is derived in Appendix A.

2. Volume averaging

In this section, we use a volume-averaging approach to get the continuum equations for acoustic flow in a porous medium. This procedure uses the averaging theorems included in Appendix B and was applied by Whitaker (1986) on equations that, even though they describe a different physical situation, are mathematically identical equations being volume averaged here.

We consider a finite volume of averaging V of the porous medium. This volume contains a liquid phase of volume V^ℓ and a solid phase of volume V^{s}, such that $V^\ell + V^{\mathrm{s}} = V$. The porosity is $\phi = V^\ell / V$. Inside V, there is a certain liquid-solid interfacial area $A^{\ell \mathrm{s}}$. The characteristic pore size is ℓ^{p}. We now wish to volume average the governing equations for $\bar{\mathbf{u}}_2$, $\bar{p}_2$ and z^i over the volume $V \sim \{\ell^{\mathrm{a}}\}^3$ to obtain macroscopic equations for the flow on the macroscopic length scale L, where the variations on the pore scale ℓ^{p} are averaged out. We must therefore, at the outset, demand that the length scale of averaging ℓ^{a} is much smaller than the linear size of the entire porous medium L and that the length scale of averaging ℓ^{a} is much larger than the pore length scale ℓ^{p}. This may be expressed as

$$\ell^{\mathrm{p}} \ll \ell^{\mathrm{a}} \ll L, \tag{22}$$

and is also illustrated in FIG. 2.

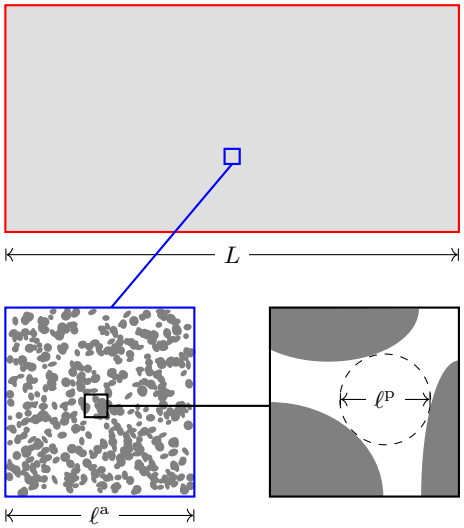

FIG. 2. Illustration of the length scales used in the volume-averaging approach. Framed in red is the entire porous material, which represents the macroscopic length scale L. Cut out from this, and framed in blue, is the volume of averaging $V \sim \{\ell^{\mathrm{a}}\}^3$. The averaging volume contains many pores and is large compared to the typical pore size ℓ^{p}. The dark gray grains represent the solid phase and the liquid phase is shown in white.

In the volume occupied by the liquid phase V^ℓ we have, from our time-averaging procedure, that $\bar{\mathbf{u}}_2$ and $\bar{p}_2$ are governed by equation (16) subject to the constraint

that $\bar{\mathbf{u}}_2$ be divergence-free (11). Furthermore, there is a no-slip boundary condition on $\bar{\mathbf{u}}_2$ at the liquid–solid interface, see Eq. (21).

We now introduce two different volume averages, the bulk average (Whitaker, 1986)

$$\langle \psi \rangle = \frac{1}{V} \int_{V^\ell} \bar{\psi} \, \mathrm{d}V^\ell, \tag{23}$$

and the phase average

$$\langle \psi \rangle^\ell = \frac{1}{V^\ell} \int_{V^\ell} \bar{\psi} \, \mathrm{d}V^\ell. \tag{24}$$

The difference between the two averages is the volume of normalization and the two are thus related by

$$\langle \psi \rangle = \phi \langle \psi \rangle^\ell. \tag{25}$$

In a porous medium where the quantity ψ is constant in the pore space, the phase average will be equal to this constant pore-space value, while the bulk average will not. For this reason, we wish that our final equations involve the phase averages $\langle p_2 \rangle^\ell$ and $\langle \mathbf{F}_2 \rangle^\ell$. For $\bar{\mathbf{u}}_2$, on the other hand, we want the bulk average since the volumetric flux is

$$\mathbf{q} = \langle \rho \mathbf{v} / \rho_0 \rangle = \langle \mathbf{u}_2 \rangle. \tag{26}$$

Applying the spatial averaging theorem (B2) to $\bar{\mathbf{u}}_2$, and using the constraint that $\bar{\mathbf{u}}_2$ is divergence free (11) along with the no-slip boundary condition (21) on $A^{\ell s}$, gives

$$\nabla \cdot \mathbf{q} = 0. \tag{27}$$

The volumetric flux resulting from acoustic streaming is thus divergence-free.

The spatial average of the second-order momentum equation (16) is

$$\langle \eta \nabla^2 \mathbf{u}_2 \rangle = \langle \nabla p_2 \rangle - \langle \mathbf{F}_2 \rangle. \tag{28}$$

As alluded to initially, our goal is to write this in terms of $\nabla \langle p_2 \rangle^\ell$, $\langle \mathbf{F}_2 \rangle^\ell$ and $\mathbf{q}$. The bulk average of $\bar{\mathbf{F}}_2$ is easily related to the phase average by (25), i.e., $\langle \mathbf{F}_2 \rangle = \phi \langle \mathbf{F}_2 \rangle^\ell$. For the pressure, we introduce the decomposition $\bar{p}_2 = \langle p_2 \rangle^\ell + \tilde{p}_2$, and use the spatial averaging theorem (B1) and also (B3), to get

$$\langle \nabla p_2 \rangle = \phi \nabla \langle p_2 \rangle^\ell + \frac{1}{V} \int_{A^{\ell s}} \tilde{p}_2 \mathbf{n} \, \mathrm{d}A^{\ell s}, \tag{29}$$

where $\mathbf{n}$ is a unit vector normal to the liquid-solid interface. For the Laplacian term in the averaged momentum equation, we apply the averaging theorem (B2) twice and use the no-slip condition (21) to eliminate the resulting integral of $\bar{\mathbf{u}}_2$ over the liquid-solid interface. This gives

$$\langle \eta \nabla^2 \mathbf{u}_2 \rangle = \eta \nabla^2 \langle \mathbf{u}_2 \rangle + \eta \frac{1}{V} \int_{A^{\ell s}} \mathbf{n} \cdot \nabla \bar{\mathbf{u}}_2 \, \mathrm{d}A^{\ell s}, \tag{30}$$

$$\approx \eta \frac{1}{V} \int_{A^{\ell s}} \mathbf{n} \cdot \nabla \bar{\mathbf{u}}_2 \, \mathrm{d}A^{\ell s}. \tag{31}$$

In the final approximation, we have used the fact that $\langle \mathbf{u}_2 \rangle$ varies on the macroscopic scale L and that $\bar{\mathbf{u}}_2$ varies on the much smaller pore scale ℓ^{p} to neglect the Laplacian of $\langle \mathbf{u}_2 \rangle$. With the above results [Eqs. (29) and (31)] for $\langle \nabla p_2 \rangle$ and $\langle \eta \nabla^2 \mathbf{u}_2 \rangle$, the spatially averaged momentum equation becomes,

$$\frac{1}{V} \int_{A^{\ell s}} \{ \eta \mathbf{n} \cdot \nabla \bar{\mathbf{u}}_2 - \tilde{p}_2 \mathbf{n} \} \, \mathrm{d}A^{\ell s} = \phi \nabla \langle p_2 \rangle^\ell - \phi \langle \mathbf{F}_2 \rangle^\ell. \tag{32}$$

A closure relation for the integral in this equation may be obtained following a mathematically identical procedure to that taken by Whitaker (1986). For an isotropic medium, we get

$$\frac{1}{V} \int_{A^{\ell s}} \{ \eta \mathbf{n} \cdot \nabla \bar{\mathbf{u}}_2 - \tilde{p}_2 \mathbf{n} \} \, \mathrm{d}A^{\ell s} \approx -\frac{\eta \phi}{\kappa} \langle \mathbf{u}_2 \rangle, \tag{33}$$

where κ is the permeability of the porous material. This result may also be obtained by arguing that the integral represents the force exerted on the solid by the slow, average movement of the liquid relative to the solid. Inserting the closure relation into (32) and solving for $\langle \mathbf{u}_2 \rangle = \mathbf{q}$, we get an equation on the same form as Darcy's law,

$$\mathbf{q} = -\frac{\kappa}{\eta} \left\{ \nabla \langle p_2 \rangle^\ell - \langle \mathbf{F}_2 \rangle^\ell \right\}, \tag{34}$$

for the volumetric flux due to acoustic streaming.

We apply spatial averaging also to the component mass balance equation (20). This procedure is, again, mathematically identical to that used by Whitaker (1985). We therefore state the result,

$$\partial_t \left\{ \phi \rho_0 \langle z^i \rangle^\ell \right\} + \nabla \cdot \left\{ \rho_0 \langle z^i \rangle^\ell \mathbf{q} \right\} = 0, \tag{35}$$

and refer to (Whitaker, 1985) for further details. We shall not consider dispersive effects here and have therefore neglected the dispersive terms in (35).

C. Model for the acoustic radiation force

The equations (27) and (34) for the time-averaged acoustic streaming on the macroscopic length scale require the acoustic radiation force to be known. This is given by the first-order acoustic fields and there are many ways to estimate them with varying levels of sophistication and complexity. It is not within the scope of this work to perform a sophisticated calculation of ultrasound propagation. We opt instead for a relatively simple approach that relies on a number of assumptions. This is done for the sake of simplicity, but it is not strictly necessary. The model equations for the acoustic streaming are equally valid with first-order fields and acoustic radiation forces calculated by more advanced methods.

For fields that are adequately directional and not highly focused, the paraxial (or parabolic) approximation is valid in the vicinity of the main propagation axis. The acoustic radiation force is then commonly approximated as (Raghavan, 2018)

$$\langle \mathbf{F}_2 \rangle^\ell = \frac{2\alpha \mathbf{I}}{c_0}, \tag{36}$$

where α is the acoustic attenuation coefficient. Furthermore, we assume that the attenuation of the applied sound wave is relatively slow and combine the plane-wave relation $\mathbf{v}_1 = p_1/(\rho_0 c_0)\ \hat{\mathbf{x}}$ with (7), to approximate the intensity as

$$\mathbf{I} = \frac{|\bar{p}_1|^2}{2\rho_0 c_0}\ \hat{\mathbf{x}}. \tag{37}$$

We assume here that the first-order fields are time-harmonic fields with a spatially varying amplitude and consider first-order pressure fields to take the form

$$p_1 = \frac{P_1}{2}\exp\left(-i\omega t\right) + \frac{P_1^*}{2}\exp\left(i\omega t\right), \tag{38}$$

where ω is the angular frequency of the sound wave, i is the imaginary unit, asterisks denote complex conjugates and P_1 is the spatially varying complex amplitude of the acoustic pressure.

There are many different models to use for the first-order pressure field (Marston, 2011a,b; O'Neil, 1949; Treeby *et al.*, 2018), but in order to have a simple expression to model the acoustic radiation force we follow the work of Prieur and Sapozhnikov (2017); Sapozhnikov (2012) who, as a solution to the Helmholtz equation, defined an axisymmetric beam with a quasi-Gaussian pressure distribution. The complex amplitude is described as

$$P_1 = \frac{P_0 x_\mathrm{d}}{2\sinh^2(k x_\mathrm{d})}\left\{ e^{k x_\mathrm{d}}\frac{\sin\left(k\sqrt{D_-}\right)}{\sqrt{D_-}} - e^{-k x_\mathrm{d}}\frac{\sin\left(k\sqrt{D_+}\right)}{\sqrt{D_+}}\right\}, \tag{39}$$

where

$$x_\mathrm{d} = k w_0^2/2, \tag{40}$$
$$D_- = (x - i x_\mathrm{d})^2 + y^2 + z^2, \tag{41}$$
$$D_+ = (x + i x_\mathrm{d})^2 + y^2 + z^2, \tag{42}$$

w_0 is a parameter characterizing the spatial extension of the beam in the plane $x = 0$ and $k = 2\pi f/c_0$ is the wavenumber, given by the ultrasound frequency f and the sound speed c_0 in the medium. We let P_0 be $P_0 = \sqrt{2\rho_0 c_0 I}$ so that the maximum value of the maximum intensity magnitude will be given by the intensity I.

D. Dimensionless equations

It is useful to cast the governing equations (27) and (34) in dimensionless form. This can be done using the three dimensionful quantities, e.g., the length w_0, the hydraulic conductivity of the porous material $K = \kappa/\eta$ and the maximum magnitude of the acoustic radiation force in the domain $F_2^{\max} = \max_{x,y,z}\left(\left|\langle \mathbf{F}_2\rangle^\ell\right|\right)$.

The relations between the dimensionless and dimensionful volumetric flux, second-order pressure and acoustic radiation force are thus

$$\mathbf{q} = K F_2^{\max}\mathbf{q}', \tag{43}$$
$$\langle p_2\rangle^\ell = w_0 F_2^{\max}\langle p_2'\rangle^\ell, \tag{44}$$
$$\langle \mathbf{F}_2\rangle^\ell = F_2^{\max}\langle \mathbf{F}_2'\rangle^\ell, \tag{45}$$

where the dimensionless quantities are indicated with a prime. Furthermore, the dimensionless versions of (27) and (34) are, respectively,

$$\nabla'\cdot\mathbf{q}' = 0, \tag{46}$$
$$\mathbf{q}' = -\left\{\nabla'\langle p_2'\rangle^\ell - \langle \mathbf{F}_2'\rangle^\ell\right\}. \tag{47}$$

If we consider a domain that is large enough compared to the focal spot, the solution to the dimensionless equations only depend on $\langle \mathbf{F}_2'\rangle^\ell$, i.e., the spatial variation of the acoustic radiation force relative to its maximum value. For the model force field used here (Section II C) this spatial variation is determined by the dimensionless parameter kw_0. From (43) and the choice of model for the acoustic radiation force in Section II C, we then get that the dimensionful flux, for a particular value of kw_0, is linearly proportional to the applied intensity I, linearly proportional to the permeability κ of the porous material, linearly proportional to the attenuation coefficient α and inversely proportional to the liquid viscosity η.

III. NUMERICAL SOLUTION PROCEDURE

Since the volumetric flux field $\mathbf{q}$ is divergence free [Eq. (27)] and is described by Eq. (34), on the same form as Darcy's law, the numerical solution procedure for calculating it is relatively straightforward.

Combining (27) and (34) gives a Poisson-type equation for $\langle p_2\rangle^\ell$,

$$\nabla\cdot\left\{\frac{\kappa}{\eta}\left\{\nabla\langle p_2\rangle^\ell - \langle \mathbf{F}_2\rangle^\ell\right\}\right\} = 0, \tag{48}$$

where $\langle \mathbf{F}_2\rangle^\ell$ is assumed known and modeled as described in Section II C. This equation is discretized on a spatial grid using the finite volume method. The discretization procedure produces a linear system of equations that can be solved numerically for $\langle p_2\rangle^\ell$ when appropriate boundary conditions are set. Here, we shall use only homogeneous Dirichlet boundary conditions, i.e., $\langle p_2\rangle^\ell = 0$. With (48) solved and $\langle p_2\rangle^\ell$ known, $\mathbf{q}$ can be calculated from (34).

In this work, we consider only cases that are rotationally symmetric around the beam axis, i.e., the x-axis. To save computational time, we therefore discretize and solve (48) in cylindrical coordinates.

IV. SIMULATIONS

In this section, we present and discuss results from simulations in a domain that is large compared to the focal spot of the beam. Also, we compare the results from the simplified expression for the acoustic streaming, used

by e.g. Manor (2021), to numerical solutions to the full equations. Following the arguments from Section II D, we present simulation results in dimensionless quantities and vary only kw_0.

Simulations were performed for different shapes of the acoustic radiation force, corresponding to a range of different values of kw_0. Two examples with $kw_0 = 3$ and $kw_0 = 6$ are shown in FIG. 3. As kw_0 increases, the focal point becomes longer in the axial direction, compared to its width, which corresponds to increasing F-number and weaker focusing of the ultrasound beam. Volumetric fluxes are shown in FIG. 4. For both force fields, the flux is largest at the focal point and quickly becomes small in magnitude away from the focal point. Near the beam axis, flow is in the axial direction, while the fluid off-axis is drawn towards the focal point on the upstream side and is pushed away from it at the downstream side. The maximum in the flux, found near the focal point, increases with kw_0.

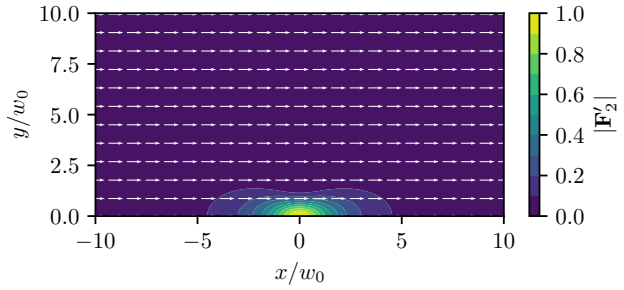

(a)

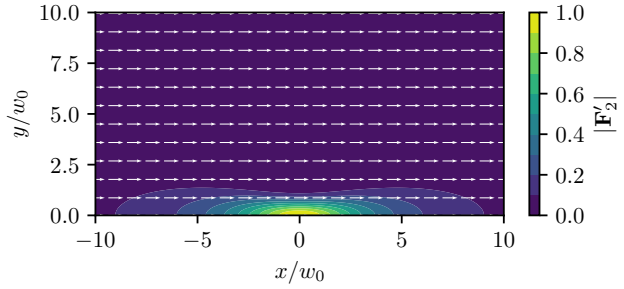

(b)

FIG. 3. Dimensionless acoustic radiation force fields with (a) $kw_0 = 3$ and (b) $kw_0 = 6$. The white arrows shows the direction of the acoustic radiation force and the contour indicates the magnitude.

Manor (2021) uses a simplified expression to estimate the acoustic streaming directly from the acoustic radiation force, without solving any equations. According to him, the contribution from the gradient in pressure will often be small compared to that from the acoustic radiation force in (34). Dropping the pressure gradient term,

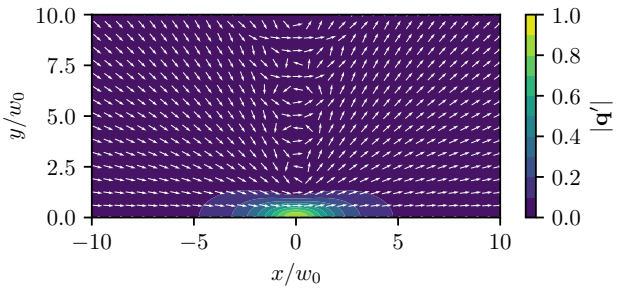

(a)

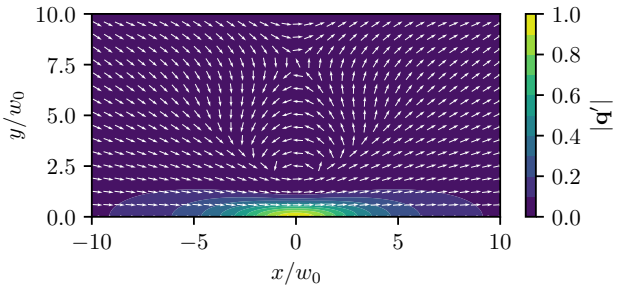

(b)

FIG. 4. Dimensionless volumetric fluxes with (a) $kw_0 = 3$, (b) $kw_0 = 6$. The white arrows shows the direction of the volumetric flux and the contour indicates the magnitude.

(34) becomes

$$\mathbf{q} \approx \frac{\kappa}{\eta}\langle \mathbf{F}_2 \rangle^{\ell}, \tag{49}$$

which is equivalently stated in dimensionless quantities as

$$\mathbf{q}' \approx \langle \mathbf{F}_2' \rangle^{\ell}. \tag{50}$$

We now investigate how this approximation compares to solutions to the full equations.

FIG. 5 shows the difference in x-component of the dimensionless volumetric flux, from the above solutions to the full equations, and the x-component of the dimensionless acoustic radiation force. FIG. 5 thus represents the errors in the x-component of (50). The simplified expression overestimates the flux at the focal point in both cases. The error decreases, however, with increasing kw_0. At $kw_0 = 3$, the maximum error is 0.1, and quite significant, while at $kw_0 = 6$ the maximum error is only 0.03.

With the simplified expression in (49), the direction of the flow is always the same as the force. Here, this is a good approximation near the beam axis, but it is qualitatively wrong further away from the axis and, e.g., in the region of back-flow seen e.g., in FIG. 4 (b), entirely in the wrong direction. The reason is that in the solutions to the full equations, (27) and (34), $\langle p_2 \rangle^{\ell}$ is determined

such as to make $\mathbf{q}$ divergence free. However, when the simplified equation (49) is used, the contribution to $\mathbf{q}$ from $\langle p_2 \rangle^\ell$ is neglected and a zero divergence of $\mathbf{q}$ is not generally obtained. In such cases, the solution does not satisfy mass conservation.

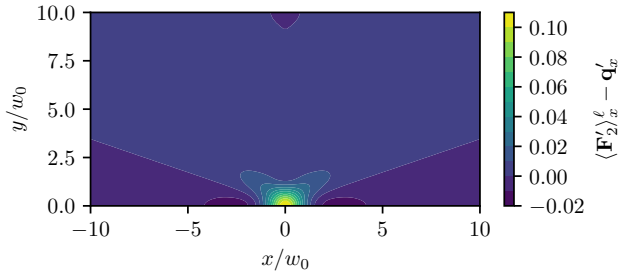

(a)

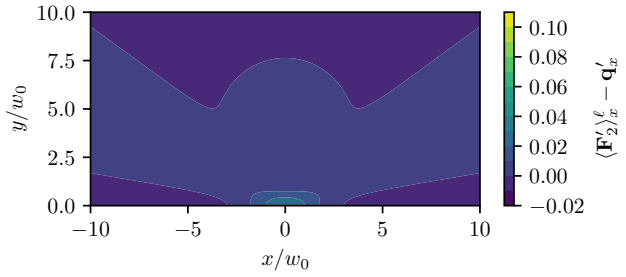

(b)

FIG. 5. Errors in x-component of (50) for (a) $kw_0 = 3$ and (b) $kw_0 = 6$. The contour indicates the magnitude.

In summary, we may conclude that (49) represents a reasonable approximation to the acoustic streaming near the beam axis for kw_0-values that are sufficiently large, corresponding to high F-numbers. For low F-numbers, Eq. (49) over-estimates the flow near the focal point and, away from the beam axis, it may predict flow in the wrong direction.

V. COMPARISON WITH EXPERIMENT

In this section we shortly summarize the experimental setup by El Ghamrawy *et al.* (2019) and then compare their results to predictions from our model. The experiments are described in detail in (El Ghamrawy, 2019) and we base our comparison on this description.

A. Experimental setup

El Ghamrawy (2019) performed experiments where a gel was subjected to focused ultrasound. The effect of the resulting acoustic streaming of water in the gel was assessed by observing the gradual removal of a dye injected near the ultrasound focal spot.

The experimental setup is illustrated in FIG. 6. A dye of 0.025 mL 0.1 % bromophenol blue was injected into a region with thickness $h = 2.42\,\mathrm{mm}$ at the surface of a piece of macroporous polyalcrylamide (MPPa) gel. The gel had porosity $\phi = 0.88$, permeability $\kappa = 6.43 \times 10^{-12}\,\mathrm{m}^2$ and was assumed to have a density $\rho_0 = 1000\,\mathrm{kg\,m^{-3}}$. Furthermore, the speed of sound was $c_0 = 1480\,\mathrm{m\,s^{-1}}$ and the ultrasound attenuation coefficient was $\alpha = 0.63\,\mathrm{Np\,m^{-1}}$ at the transducer frequency $f = 5\,\mathrm{MHz}$. The gel was immersed in a tank with degassed water and the dyed MPPa surface was placed normal to the beam axis, 35 mm away from the transducer. Thus, the gel occupied the proximal half of the focal volume while water was in the distal half. The size of the focal region was given by the full width half maximum, $\mathrm{FWHM}_x = 3.2\,\mathrm{mm}$ and $\mathrm{FWHM}_y = 0.45\,\mathrm{mm}$.

Using this setup for three different spatial peak time average intensities I_{SPTA} of $159\,\mathrm{W\,cm^{-2}}$, $646\,\mathrm{W\,cm^{-2}}$ and $1317\,\mathrm{W\,cm^{-2}}$, El Ghamrawy (2019) captured the change in light intensity transmitted through the dyed region, the dye clearance, with a camera over a period of 30 s of ultrasound exposure. The resulting dye clearance curves are shown in FIG. 7.

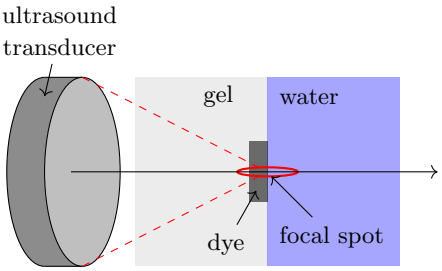

FIG. 6. An illustration of the experimental setup by El Ghamrawy (2019). The MPPa gel is shown as the light gray area with a localized area of a dye indicate by dark gray. The water tank is shown in blue. The setup was sonicated with a 5 MHz focused ultrasound transducer illustrated on the left-hand side.

B. Extracting volumetric fluxes from the experimental data

The experiments by El Ghamrawy (2019) do not measure acoustic streaming directly, but rather the change in optical intensity in the area of the dyed region corresponding to the FWHM_y of the ultrasound pressure field. In this section, we give a procedure to extract volumetric fluxes from the experiments using the transport equation (35). We also give the values of the extracted volumetric fluxes.

Consider a cylindrical control volume aligned with the beam axis and with cross-sectional area A, given by the beam FWHM_y, and length h along the beam axis equal to the thickness of the injected layer of dye. Integrating the volume-averaged mass equation (35) for the

dye (d) over this control volume gives

$$\frac{1}{Ah}\int \left\{\rho_0 \partial_t \left\{\phi\langle z^{\mathrm{d}}\rangle^{\ell}\right\} + \rho_0 \nabla\cdot\left\{\langle z^{\mathrm{d}}\rangle^{\ell}\mathbf{q}\right\}\right\} \mathrm{d}V = 0. \quad (51)$$

We approximate $\phi\langle z^{\mathrm{d}}\rangle^{\ell}$ as spatially uniform within the control volume so that

$$\frac{1}{Ah}\int \rho_0 \partial_t \left\{\phi\langle z^{\mathrm{d}}\rangle^{\ell}\right\} \mathrm{d}V \approx \partial_t \left\{\rho_0\phi\langle z^{\mathrm{d}}\rangle^{\ell}\right\}. \quad (52)$$

When the acoustic streaming starts, we assume $\mathbf{q}$ to be roughly aligned with the beam axis within the control volume and the flux of dye is then non-zero only through the downstream end. Using the divergence theorem, we then get

$$\frac{1}{Ah}\int \rho_0 \nabla\cdot\left\{\langle z^{i}\rangle^{\ell}\mathbf{q}\right\} \mathrm{d}V = -\frac{1}{Ah}\int \rho_0\langle z^{i}\rangle^{\ell}\mathbf{q}\cdot\mathrm{d}\mathbf{A}, \quad (53)$$

$$\approx -\frac{\rho_0\phi\langle z^{i}\rangle^{\ell}q_A}{\phi h} \quad (54)$$

where q_A is the averaged volumetric flux across the downstream end of the control volume,

$$q_A = \frac{1}{A}\int \mathbf{q}\cdot\mathbf{x}\,\mathrm{d}A. \quad (55)$$

We now define the density of dye in the control volume as $\zeta = \rho_0\phi\langle z^{\mathrm{d}}\rangle^{\ell}$. With the assumptions above, (51) then becomes an ordinary differential equation (ODE) for ζ,

$$\partial_t\zeta = -\frac{q_A}{\phi h}\zeta. \quad (56)$$

This ODE has the solution

$$\zeta(t) = \zeta_0 \exp\left(-\frac{q_A t}{\phi h}\right), \quad (57)$$

where ζ_0 is the initial density of dye in the control volume.

The optical intensity measured in the FWHM may be assumed to be linearly proportional to the density of dye in our control volume. The dye clearance curves presented in El Ghamrawy (2019), i.e., the reduction in optical intensity at time t relative to the initial optical intensity, should therefore be equal to

$$\frac{\zeta_0 - \zeta(t)}{\zeta_0} = 1 - \exp\left(-\frac{q_A t}{\phi h}\right). \quad (58)$$

Since ϕ and h are known, we can fit this equation to the dye clearance curves by adjusting the single parameter q_A. Fitted curves for each of the three different ultrasound intensities applied are shown in FIG. 7 and they agree very well with the measured curves. The fitting procedure thus gives the value of q_A for each intensity and the resulting values are $5.96\,\mu\mathrm{m\,s^{-1}}$ $21.1\,\mu\mathrm{m\,s^{-1}}$ and $63.9\,\mu\mathrm{m\,s^{-1}}$ for intensities of $159\,\mathrm{W\,cm^{-2}}$, $646\,\mathrm{W\,cm^{-2}}$ and $1317\,\mathrm{W\,cm^{-2}}$, respectively.

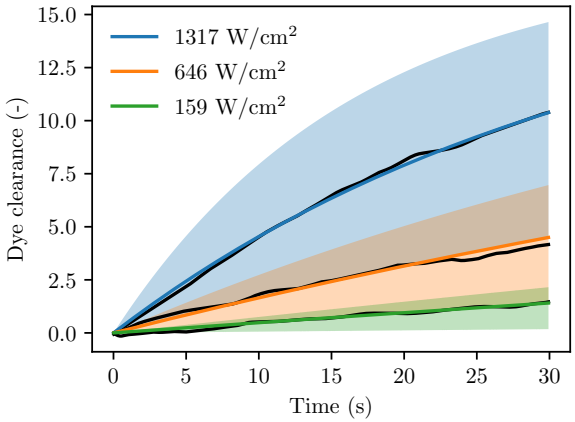

FIG. 7. Dye clearance curves measured by El Ghamrawy (2019) for different ultrasound beam intensities (black lines). To each experiment a fit to (58) was made and these are shown as blue, orange and green lines. The shaded areas represent the uncertainties in the fitted lines due to the experimental uncertainties given in (El Ghamrawy, 2019).

C. Comparison between experimental and predicted fluxes

In this section we compare the FWHM-averaged volumetric fluxes q_A, as predicted by the model we have presented, with those extracted from the experiments of El Ghamrawy (2019) in the preceding section.

We neglected any temperature and non-linear effects and used the quasi-Gaussian beam (36) again as the model force field for the simulations. The wavenumber $k = 2\pi f/c_0$ is given by the ultrasound frequency f and the sound speed c_0 in the gel. The parameter w_0 was set such that the experimentally measured value of FWHM_y was obtained for the model field. With w_0 determined, FWHM_x for the model beam was found to be 2.6 mm. This represents a relatively small deviation of about 19 % from the experimental value of 3.2 mm. The resulting kw_0-value for the model field was 5.6. The parameter P_0 was set such as to get the same intensity used in the experiments, as described in Section II C. In this case it was the same as I_{SPTA} from the experiments since the duty cycle was at 100 %. The dynamic viscosity η was not given in the work of El Ghamrawy (2019), and we assumed the value to be similar to that of water and set it to $\eta = 0.001\,\mathrm{Pa\,s}$.

Since the attenuation coefficient α is much lower in the water than in the gel (El Ghamrawy, 2019), we expect the acoustic radiation force and the gradients in $\langle p_2\rangle^{\ell}$ in the water to be small compared to the gel. The computational domain in the simulations was therefore limited to the gel and a Dirichlet boundary condition $\langle p_2\rangle^{\ell} = 0$ was set on the gel-water boundary. The other boundaries were placed far away from the focal point and $\langle p_2\rangle^{\ell} = 0$ was set there also.

The simulated acoustic radiation force, second-order pressure and volumetric flux fields for the $646\,\mathrm{W\,cm^{-2}}$

case are shown in FIG. 8. The acoustic streaming shown in FIG. 8 (c) is fastest near the focal point and is, in much of the domain shown, closely aligned with the beam axis. The second-order pressure field as shown in FIG. 8 (b), however, contributes to some movement of fluid towards the focal point.

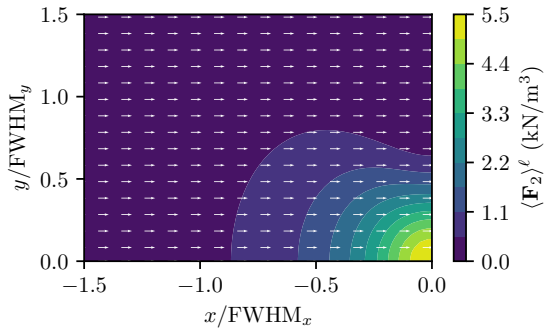

(a)

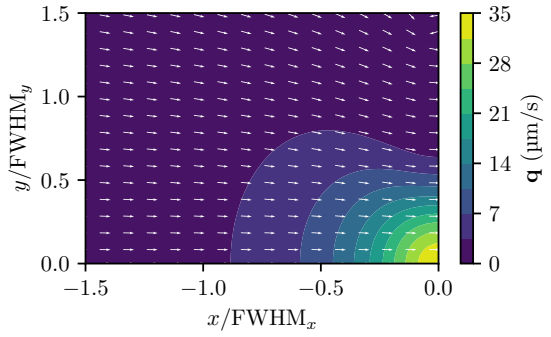

(b)

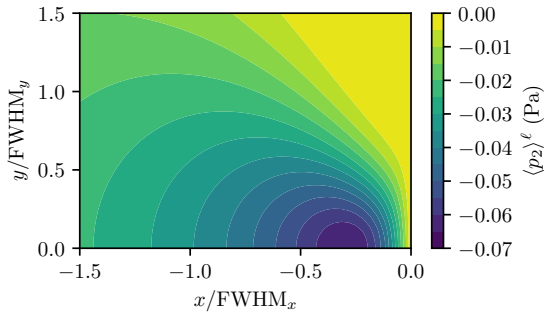

(c)

FIG. 8. Simulation results for (a) acoustic radiation force, (b) second-order pressure and (c) volumetric flux for the El Ghamrawy (2019) case with $I_{\mathrm{SPTA}} = 646\,\mathrm{W\,cm^{-2}}$.

The x-component of the dimensionless volumetric flux $\mathbf{q}'_x$ from this case, along the gel-water interface at $x = 0$, is shown in FIG. 9. Also shown is the dimensionless acoustic radiation force $\langle \mathbf{F}'_2 \rangle^\ell_x$ which represents the approximation of the dimensionless volumetric flux given by (50). The lines representing $\mathbf{q}'_x$ and $\langle \mathbf{F}'_2 \rangle^\ell_x$ agree well and indicate that (50) is a reasonable approximation to the volumetric flux in this case.

From each of the curves representing $\mathbf{q}'_x$ and $\langle \mathbf{F}'_2 \rangle^\ell_x$, shown in FIG. 9, the dimensionless FWHM-averaged volumetric flux was calculated by numerical integration of (55) over the FWHM. The averaged values obtained by this procedure are indicated by solid lines in FIG. 9. The dimensionless fluxes were subsequently translated to dimensionful fluxes by multiplying with $KF_2^{\max}$, see Eq. (43).

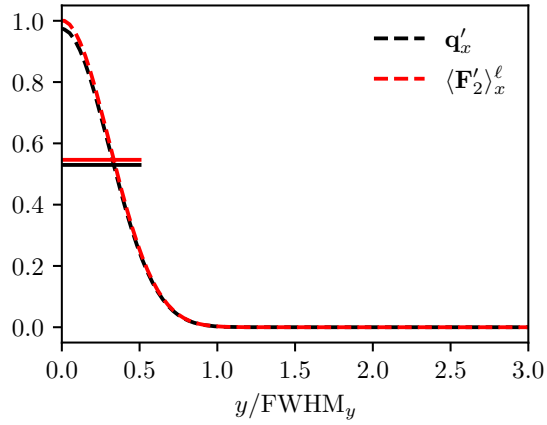

FIG. 9. The x-component of the dimensionless volumetric flux (black dashed line) and the dimensionless acoustic radiation force (red dashed line) along the y-axis at $x = 0$. The black and red horizontal lines indicate the FWHM-averaged values of the volumetric flux and the acoustic radiation force respectively.

Since the dimensionful volumetric fluxes are linear in $F_2^{\max}$ they are also linear in I_{SPTA}. The model therefore predicts the linear dashed lines shown in FIG. 10 when plotting the FWHM-averaged volumetric fluxes against the intensity. Also shown in FIG. 10 are the FWHM-averaged fluxes extracted from the experiments of El Ghamrawy (2019). The predictions from the full model (dashed black lines) is within the uncertainty of the experimental results and there is good agreement between them for the two lower intensities. The same is also true when using the approximation (50) to get predictions from the model (dashed red lines). For the high ultrasound intensity $I_{\mathrm{SPTA}} = 1317\,\mathrm{W\,cm^{-2}}$ the model results are well within the experimental uncertainty, but seem to underpredict the average experimental value. This could be related to temperature effects of the ultrasound, e.g., a decrease in liquid viscosity when the gel is heated, or non-linear effects of ultrasound propagation. These effects have not been accounted for here, but including them in the model could be a topic for future work.

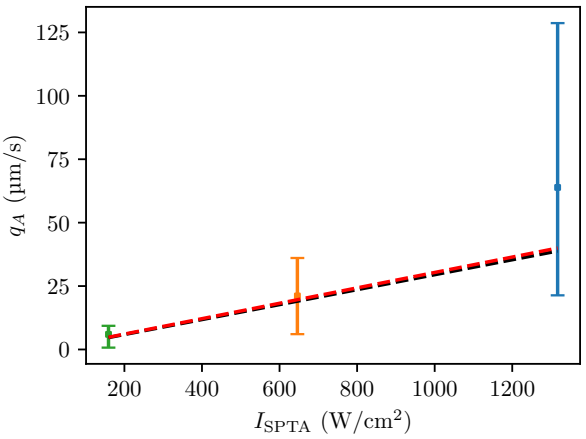

FIG. 10. FWHM-averaged volumetric fluxes for different ultrasound beam intensities (blue, orange and green squares) extracted from the experiments by El Ghamrawy (2019). The FWHM-averaged volumetric fluxes predicted by the model are shown as the dashed black line. The red dashed line indicates the FWHM-averaged volumetric flux obtained using the approximation (50).

In summary, the presented model for acoustic streaming agrees well with the experiments of El Ghamrawy (2019) and predicts results for the FWHM-averaged volumetric flux that are well within the experimental uncertainties.

VI. CONCLUSIONS

We have derived and presented equations describing acoustic streaming in soft porous media driven by focused ultrasound. The derivations were based on the assumption that acoustic waves pass through the porous material as if it were homogeneous and the resulting equations predict the time-averaged flow on the macroscopic scale. We have also stated a time- and volume-averaged equation advective transport of trace components.

Using the presented model, we performed simulations for different shapes of the focused ultrasound beam, characterized by the dimensionless parameter kw_0. Herein, k is the ultrasound wavenumber and w_0 is a parameter characterizing the beam width. For a particular beam shape, and using the paraxial approximation for the ultrasound, the acoustic streaming was linearly proportional to the applied ultrasound intensity, to the permeability of the porous material and to the attenuation coefficient, and inversely proportional to the liquid viscosity.

Results from simulations were compared to a simplified expression for the acoustic streaming stating that the dimensionless volumetric flux is equal to the dimensionless acoustic radiation force. This was found to represent a reasonable approximation to the acoustic streaming near the beam axis for kw_0-values that were sufficiently large, corresponding to high F-numbers. For low F-numbers, the simplified expression over-estimates the flow near the focal point and, away from the beam axis, it may predict flow in the wrong direction.

Finally, the presented model for acoustic streaming was compared to experimental results from El Ghamrawy *et al.* (2019) and was found to agree well. The model-predicted volumetric fluxes, averaged over the beam FWHM, were within the experimental uncertainties.

In the future, we hope that the model can be used to interpret experimental results relevant for enhanced drug delivery in tissue, and to assess the relative importance of acoustic streaming compared with other effects.

ACKNOWLEDGMENTS

The authors would like to thank James Choi at Imperial College London for very helpful correspondence and Caroline Einen, Anders Lervik, Catharina Davies and Signe Kjelstrup at the Norwegian University of Science and Technology and Robin Cleveland at the University of Oxford for fruitful discussions. The work was supported by the The Research Council of Norway through project 301581 and through its Centre of Excellence funding scheme, project number 262644, PoreLab.

APPENDIX A: NO-SLIP ON LIQUID-SOLID BOUNDARY

Due to viscosity, the fluid and solid velocities must be equal at their common interface, i.e. $\mathbf{v} = \mathbf{v}^{\mathrm{s}}$ on $A^{\ell \mathrm{s}}$. Since $\mathbf{v}_1 = \mathbf{v}_1^{\mathrm{s}}$ everywhere by the homogeneous medium assumption (Manor, 2021), then

$$\bar{\mathbf{v}}_2 = \bar{\mathbf{v}}_2^{\mathrm{s}} \text{ on } A^{\ell \mathrm{s}}. \tag{A1}$$

Using (6) and (10), we get

$$\bar{\mathbf{u}}_2 = \frac{\overline{\rho_1 \mathbf{v}_1}}{\rho_0} - \frac{\overline{\rho_1^{\mathrm{s}} \mathbf{v}_1^{\mathrm{s}}}}{\rho_0^{\mathrm{s}}} \text{ on } A^{\ell \mathrm{s}}. \tag{A2}$$

We will now argue that, under the homogeneous medium assumption employed here, the right hand side of (A2) is zero.

Within a small region in the immediate vicinity of the interface we can assume isentropic first-order fields. Attenuation of the sound wave occurs at a much larger length scale. The density is then, to first order,

$$\rho = \rho_0 + \rho_1 = \rho_0 + \left(\frac{\partial \rho}{\partial p}\right)_s p_1, \tag{A3}$$

The first-order perturbations in pressure and density are therefore related through

$$p_1 = c_0^2 \rho_1, \tag{A4}$$

where $c_0 = \sqrt{(\partial p/\partial \rho)_s}$ is the speed of sound. The intensity defined in (7) can be written as

$$\mathbf{I} = c_0^2 \, \overline{\rho_1 \mathbf{v}_1}. \tag{A5}$$

According to the homogeneous medium assumption, the sound waves propagate from the liquid to the solid as if it were a homogeneous medium. Specifically, this means that the intensity must be the same at a point close to the interface and at a point immediately next to it, but on the other side. Since we have also assumed $\rho_0 = \rho_0^{\mathrm{s}}$ and $c_0 = c_0^{\mathrm{s}}$, then the right-hand-side of (A2) must be zero.

We have here treated the solid as if it were a fluid. This is reasonable under the approximation used here, that shear waves are relatively unimportant, see e.g., (LeVeque, 2002, pp. 498–499).

APPENDIX B: SPATIAL AVERAGING THEOREM

For reference, we here state the spatial averaging theorem used in Section II B 2. For a scalar ψ, this takes the form (Whitaker, 1986)

$$\langle \nabla \psi \rangle = \nabla \langle \psi \rangle + \frac{1}{V} \int_{A^{\ell \mathrm{s}}} \bar{\psi} \mathbf{n} \, \mathrm{d}A^{\ell \mathrm{s}}, \tag{B1}$$

and, for a vector $\mathbf{A}$,

$$\langle \nabla \cdot \mathbf{A} \rangle = \nabla \cdot \langle \mathbf{A} \rangle + \frac{1}{V} \int_{A^{\ell \mathrm{s}}} \mathbf{n} \cdot \bar{\mathbf{A}} \, \mathrm{d}A^{\ell \mathrm{s}}. \tag{B2}$$

A special case is obtained when averaging over the gradient of the constant scalar 1. This gives

$$\frac{1}{V} \int_{A^{\ell \mathrm{s}}} \mathbf{n} \, \mathrm{d}A^{\ell \mathrm{s}} = -\nabla \phi. \tag{B3}$$

Afadzi, M., Myhre, O. F., Yemane, P. T., Bjørkøy, A., Torp, S. H., van Wamel, A., Lelu, S., Angelsen, B. A., and de Lange Davies, C. (**2020**). "Effect of acoustic radiation force on the distribution of nanoparticles in solid tumors," IEEE Transactions on Ultrasonics, Ferroelectrics, and Frequency Control **68**(3), 432–445, doi: 10.1109/TUFFC.2020.3027072.

Brinkman, H. C. (**1949**). "A calculation of the viscous force exerted by a flowing fluid on a dense swarm of particles," Flow, Turbulence and Combustion **1**, 27, doi: 10.1007/BF02120313.

El Ghamrawy, A. (**2019**). "Acoustic streaming in soft tissue-mimicking materials," Ph.D. thesis, Department of Bioengineering, Imperial College London, UK.

El Ghamrawy, A., de Comtes, F., Koruk, H., Mohammed, A., Jones, J. R., and Choi, J. J. (**2019**). "Acoustic streaming in a soft tissue microenvironment," Ultrasound in Medicine & Biology **45**(1), 208–217, doi: 10.1016/j.ultrasmedbio.2018.08.026.

Gjennestad, M. Aa., Winkler, M., and Hansen, A. (**2020**). "Pore network modeling of the effects of viscosity ratio and pressure gradient on steady-state incompressible two-phase flow in porous media," Transport in Porous Media **132**(2), 355–379, doi: 10.1007/s11242-020-01395-z.

Landau, L. D., and Lifshitz, E. M. (**1987**). *Fluid mechanics*, **6** of *Course of Theoretical Physics*, 2 ed. (Butterworth–Heinemann Oxford, UK), Chap. I, p. 2 and Chap. II, 44–46, trans. by J. B. Sykes and W. H. Reid.

LeVeque, R. J. (**2002**). *Finite volume methods for hyperbolic problems* (Cambridge University Press, Cambridge, UK).

Lewis, G. K., Schulz, Z. R., Pannullo, S. C., Southard, T. L., and Olbricht, W. L. (**2012**). "Ultrasound-assisted convection-enhanced delivery to the brain in vivo with a novel transducer cannula assembly," Journal of Neurosurgery **117**, 1128–1140, doi: 10.3171/2012.7.JNS11144.

Lighthill, J. (**1978**). "Acoustic streaming," Journal of Sound and Vibration **61**(3), 391–418, doi: 10.1016/0022-460X(78)90388-7.

Løvmo, M. K., Yemane, P. T., Bjørkøy, A., Hansen, R., Cleveland, R., Angelsen, B., and de Lange Davies, C. (**2020**). "Effect of acoustic radiation force on displacement of nanoparticles in collagen gels," IEEE Transactions on Ultrasonics, Ferroelectrics, and Frequency Control doi: 10.1109/TUFFC.2020.3006762.

Manor, O. (**2021**). "Acoustic flow in porous media," Journal of Fluid Mechanics **920**, A11, doi: 10.1017/jfm.2021.436.

Marston, P. L. (**2011**a). "Quasi-gaussian beam analytical basis and comparison with an alternative approach (l)," The Journal of the Acoustical Society of America **130**, 1091–1094, doi: 10.1121/1.3614545.

Marston, P. L. (**2011**b). "Quasi-gaussian bessel-beam superposition: Application to the scattering of focused waves by spheres," The Journal of the Acoustical Society of America **129**, 1773–1782, doi: 10.1121/1.3559704.

Nieminen, H. J., Herranen, T., Kananen, V., Hacking, S. A., Salmi, A., Karppinen, P., and Haeggstrom, E. (**2012**). "Ultrasonic transport of particles into articular cartilage and subchondral bone," in *2012 IEEE International Ultrasonics Symposium*, pp. 1869–1872, doi: 10.1109/ULTSYM.2012.0469.

Nieminen, H. J., Ylitalo, T., Suuronen, J.-P., Rahunen, K., Salmi, A., Saarakkala, S., Serimaa, R., and Hæggström, E. (**2015**). "Delivering agents locally into articular cartilage by intense MHz ultrasound," Ultrasound in Medicine and Biology **41**, 2259–2265, doi: 10.1016/j.ultrasmedbio.2015.03.025.

Nyborg, W. L. (**1953**). "Acoustic streaming due to attenuated plane waves," The Journal of the Acoustical Society of America **25**(1), 68–75, doi: 10.1121/1.1907010.

Olbricht, W., Sistla, M., Ghandi, G., Lewis, G., and Sarvazyan, A. (**2013**). "Time-reversal acoustics and ultrasound-assisted convection-enhanced drug delivery to the brain," The Journal of the Acoustical Society of America **134**, 1569–1575, doi: 10.1121/1.4812879.

O'Neil, H. T. (**1949**). "Theory of focusing radiators," The Journal of the Acoustical Society of America **21**, 516–526, doi: 10.1121/1.1906542.

Prieur, F., and Sapozhnikov, O. A. (**2017**). "Modeling of the acoustic radiation force in elastography," The Journal of the Acoustical Society of America **142**(2), 947–961.

Raghavan, R. (**2018**). "Theory for acoustic streaming in soft porous matter and its applications to ultrasound-enhanced convective delivery," Journal of Therapeutic Ultrasound **6**(1), doi: 10.1186/s40349-018-0114-6.

Sapozhnikov, O. A. (**2012**). "An exact solution to the Helmholtz equation for a quasi-Gaussian beam in the form of a superposition of two sources and sinks with complex coordinates," Acoustical Physics **58**(1), 41–47, doi: 10.1134/S1063771012010216.

Snipstad, S., Vikedal, K., Maardalen, M., Kurbatskaya, A., Sulheim, E., and de Lange Davies, C. (**2021**). "Ultrasound and microbubbles to beat barriers in tumors: Improving delivery of nanomedicine," Advanced Drug Delivery Reviews **177**, 113847, doi: 10.1016/j.addr.2021.113847.

Treeby, B. E., Budisky, J., Wise, E. S., Jaros, J., and Cox, B. T. (**2018**). "Rapid calculation of acoustic fields from arbitrary continuous-wave sources," The Journal of the Acoustical Society of America **143**, 529–537, doi: 10.1121/1.5021245.

Wessapan, T., and Rattanadecho, P. (**2020**). "Acoustic streaming effect on flow and heat transfer in porous tissue during exposure to focused ultrasound," Case Studies in Thermal Engineering **21**, 100670, doi: 10.1016/j.csite.2020.100670.

Whitaker, S. (**1985**). "A simple geometrical derivation of the spatial averaging theorem," Chemical Engineering Education **19**(1), 18–21 and 50–52.

Whitaker, S. (**1986**). "Flow in porous media I: A theoretical derivation of Darcy's law," Transport in Porous Media **1**(1), 3–25, doi: 10.1007/BF01036523.

Yuan, B. (**2022**). "Interstitial fluid streaming in deep tissue induced by ultrasound momentum transfer for accelerating nanoagent transport and controlling its distribution," Physics in Medicine & Biology **67**, 175011, doi: 10.1088/1361-6560/ac88b5.